Title
XMM-NEWTON SURVEY OF LOCAL ABSORPTION LINES IN THE SPECTRA OF ACTIVE GALACTIC NUCLEI

Journal
The Astrophysical Journal Supplement Series, 217(2)

ISSN
0067-0049

Authors
Fang, Taotao
Buote, David
Bullock, James
et al.

Publication Date
2015-04-01

DOI
10.1088/0067-0049/217/2/21

Peer reviewed

XMM-Newton Survey of Local O VII Absorption Lines in the Spectra of Active Galactic Nuclei

Taotao Fang[1], David Buote[2], James Bullock[2], Renyi Ma[1]

ABSTRACT

Highly ionized, $z = 0$ metal absorption lines detected in the X-ray spectra of background active galactic nuclei (AGNs) provide an effective method to probe the hot ($T \sim 10^6$ K) gas and its metal content in and around the Milky Way. We present an all-sky survey of the K_α transition of the local O VII absorption lines obtained by Voigt-profile fitting archival *XMM*-Newton observations. A total of 43 AGNs were selected, among which 12 are BL Lac-type AGNs, and the rest are Seyfert 1 galaxies. At above the 3σ level the local O VII absorption lines were detected in 21 AGNs, among which 7 were newly discovered in this work. The sky covering fraction, defined as the ratio between the number of detections and the sample size, increases from at about 40% for all targets to 100% for the brightest targets, suggesting a uniform distribution of the O VII absorbers. We correlate the line equivalent width with the Galactic coordinates and do not find any strong correlations between these quantities. Some AGNs have warm absorbers that may complicate the analysis of the local X-ray absorber since the recession velocity can be compensated by the outflow velocity, especially for the nearby targets. We discuss the potential impact of the warm absorbers on our analysis. A comprehensive theoretical modeling of the X-ray absorbers will be presented in a later paper.

Subject headings: quasars: absorption lines

1. Introduction

Since the launch of the *Chandra* and *XMM*-Newton X-ray Observatories, a number of $z \sim 0$ absorption lines, produced by highly ionized metal species, were detected in the spectra of background active galactic nuclei (see, e.g., Nicastro et al. 2002; Fang et al. 2002; Rasmussen et al. 2003). These highly ionized metal absorption lines, mostly in the form of O VII and with a column density on the order of $\sim 10^{16}\mathrm{cm}^{-2}$, imply a hot, metal enriched gas distribution in and around

[1]Department of Astronomy and Institute for Theoretical Physics and Astrophysics, Xiamen University, Xiamen, Fujian 361005, China; fangt@xmu.edu.cn

[2]Department of Physics & Astronomy, 4129 Frederick Reines Hall, University of California, Irvine, CA 92697, U.S.A.

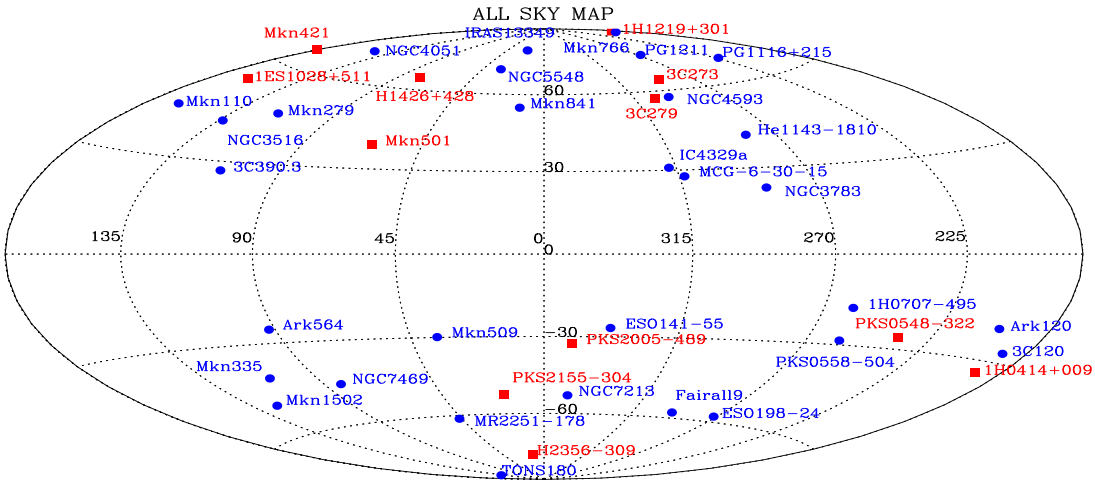

Fig. 1.— All-sky Hammer-Aitoff projection of our targets in the Galactic coordinates. Red squares are BL Lac-type targets, and blue circles are Seyfert 1 galaxies.

our Galaxy. It stirs a great amount of interest for the potential impact on our understanding of galaxy formation and evolution.

However, ever since the first detection, a crucial debate is the origin of the X-ray absorbers. For the local absorption lines seen in the quasar spectra, even with the high resolution spectrometers on-board *Chandra* and *XMM*-Newton, we can only limit the location of the absorbers to within a few Mpc, therefore it is still unclear whether this gas is associated with our disk, an extended galactic halo (Wang et al. 2006; Fang et al. 2006), or even permeates the Local Group in the form of the intragroup medium (e.g., Nicastro et al. 2002; Williams et al. 2005). Identifying the origin of this gas has significant implications on many fronts. A disk origin would benefit the study of the three-phase model of the interstellar medium (ISM, Ostriker & McKee 1978). If the absorption is produced by the hot, circumgalactic medium (CGM) in the distant halo, it would imply a significant reservoir of baryons may account for the "missing Galactic baryons" (see, e.g., Fang et al. 2006; Gupta et al. 2012). Furthermore, the hot gas could reside in the hot intergroup medium in the Local Group, which would potentially explain the so-called warm-hot intergalactic medium (WHIM, see, e.g, Nicastro et al. 2002).

The existence of the hot gas in and around the Milky Way has long been established through the observations of the soft X-ray background emission (see, e.g., McCommon & Sanders 1990; Wang & Yu 1995; Snowden et al. 1998; Kuntz & Snowden 1998; Galeazzi et al. 2007; Henley &

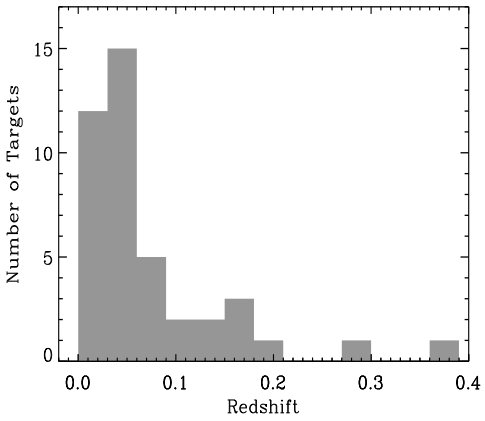

Fig. 2.— Redshift distribution of the sample AGNs.

Shelton 2008, 2013; Yoshino et al. 2009). However, current data cannot distinguish between a disk and a halo origin of the X-emitting gas. While most studies have argued for a disk morphology of the hot gas (see, e.g., Yao & Wang 2007; Hagihara et al. 2010), other studies have suggested that a halo origin is also possible (Fang et al. 2013; Henley & Shelton 2013).

Substantial progress has been made since these absorbers were first identified. McKernan et al. (2004) studied the *Chandra* spectra of 15 type I AGNs and argued that the observed metal absorption lines should be local to our Galaxy instead of high velocity outflows intrinsic to the AGNs. Fang et al. (2006) further investigated 20 AGNs from both *Chandra* and *XMM*-Newton observations and concluded the absorption line systems must be in/around the Milky Way instead of in the intragroup medium of the distant Local Group. Bregman & Lloyd-Davies (2007) reached a similar conclusion by studying the correlation between the X-ray absorption line strength and the *ROSAT* background emission measure. Furthermore, based on a survey of 26 AGNs, Bregman & Lloyd-Davies (2007) and Miller & Bregman (2013) analyzed the structure of the CGM and argued that the hot gas accounts for at most 10-50% of the missing Galactic baryons.

Despite all the progress, a critical, unresolved issue is still the relative contribution of the disk and the distant halo to the observed absorption seen in X-ray. Inspired by the disk morphology of the X-ray emission of nearby galaxies, several authors (see, e.g., Yao et al. 2009; Hagihara et al. 2010) argued that most of the X-ray absorbing gas is confined within a few kpc of the Milky Way disk. X-ray absorption lines were also detected in the nearby Galactic X-ray binaries (see, e.g., Miller et al. 2004; Yao & Wang 2005). Such absorption lines have been compared with those detected in the AGNs to determine the relative contribution of the disk and halo (see, e.g., Wang et al. 2005; Yao & Wang 2007). However, A complication arises in these studies because the X-ray absorpriton lines in the XRBs may be contaminated by the circumstellar medium intrinsic to the XRBs (Miller et al. 2004; Cackett et al. 2008). While a disk origin for the hot gas is attractive, a

halo-origin cannot be definitely excluded (see, e.g., Fang et al. 2006; Gupta et al. 2012; Miller & Bregman 2013, but also see Wang & Yao 2012).

Analysis of the complete global distribution of the $z \sim 0$ absorbers becomes necessary to resolve these issues. We have performed a comprehensive analysis of all the available data in the *XMM*-Newton archive. Our targets include a total of 43 AGNs. In this first paper, we present the results of our data analysis. We also report the first detection of $z \sim 0$ O VII absorption lines in 7 background AGNs at more than the 3σ level. Prior to this work, the most comprehensive study was performed by Miller & Bregman (2013). Their sample includes 26 AGNs, and 10 targets showed $z \sim 0$ O VII absorption lines at more than the 3σ level. Therefore our work is a significant increase in both the sample size and the newly detections of $z \sim 0$ O VII absorption lines.

This paper is organized as follows. In section §2 we describe the observations and data analysis procedures. We present our main results in this section. We discuss the consistency of our data analysis by comparing our work with previous studies in section §3, as well as the impact of warm absorbers in some Seyfert 1 galaxies. We also comment on several targets with newly detected, $z \sim 0$ O VII lines in this section. The last section provides a summary.

2. Observations and Data Analysis

2.1. Target Selection

Three high resolution X-ray spectrometers are suitable for the study of the narrow X-ray absorption lines: the low and high energy transmission gratings (LETG and HETG)[1] on-board the *Chandra* X-ray Observatory, and the The Reflection Grating Spectrometer (RGS)[2] on-board the *XMM*-Newton X-ray Telescope. We focus on the RGS data mainly due to its high collecting area at the wavelength region we are interested in. There are two RGS units: RGS 1 and RGS 2. However, due to operation failures the CCD 7 of RGS 1 and CCD 4 of RGS 2 are not working. Particularly, the CCD 4 of RGS 2 covers the He-like oxygen region which is our primary focus in this paper. Therefore in this work we will focus on the RGS 1 unit only.

The $z = 0$ X-ray absorption lines from various ion species have been reported previously. These lines were produced by metal species in a variety of ionization stages, ranging from neutral to the H-like. Most reported ion species are Ne IX at 13.44 Å, O VIII at 18.98 Å, and O VII at 21.6 Å (see, e.g, Nicastro et al. 2002; Fang et al. 2002; Rasmussen et al. 2003; Williams et al. 2005). In this work, we will mainly focus on highly ionized metals, in particular the He-like oxygen, O VII, for several reasons. First, Ne IX K_α is located in a region where the RGS 1 has no effective area, and also there are several bad pixels near the O VIII K_α region. Second, Under collisional ionization,

[1]See http://asc.harvard.edu/

[2]See http://xmm.esa.int/

the temperature for the peak O VII fraction is between $10^{5.5}$–$10^{6.5}$ degrees, providing an effective way to probe the hot gas in and around the Milky Way.

We searched the entire *XMM*-Newton archive of the AGNs with enough RGS photon counts to warrant a spectral analysis. The RGS resolution has a full width of half maximum (FWHM) of ~ 50 mÅ. We define one resolution element as half of the FWHM, or 25 mÅ. Our past experience indicates that the minimum requirement for a useful spectral fit is that the counts per resolution element, or CPRE, must be at least 20 photons. This selection criterion results in a total of 43 AGNs in our sample. Among them 12 are BL Lac-type target. The remaining 31 are various Seyfert galaxies with a subclass of between 1 and 1.5. For convenience we broadly categorize them as Seyfert 1 AGNs[3]. In Figure 1 we plot the all-sky Hammer-Aitoff projection of our targets in the Galactic coordinate. In Table 1 we list basic properties of these targets. Column (1) is the target name. Column (2) lists the AGN types. We broadly divide the entire sample into BL Lac targets (Type 1) and Seyfert 1 Galaxies (Type 2). Columns (3), (4), and (5) are the Galactic latitude, longitude and redshift, respectively. Column (6) is the Galactic neutral hydrogen column density (Dickey & Lockman 1990). Columns (7) and (8) are the total exposure time (in units of *ksec*) and the CPRE. Columns (9) – (15) are line parameters which will be described in detail later. Columns (9), (10), (11) are the O VII column density, the Doppler-b parameter, and the velocity shift of the line center, respectively. Columns (12) (13), and columns (15), (16) are the line line equivalent width (EW) and the signal-to-noise ratio (S/N) of the detection, for two different evaluation methods, respectively. We do not list the line parameters (denoted as "...") if the line is not detected (defined as the S/N falls below 1), except the 3σ upper limits of the EW. We also list the C-statistic and degree of freedom in column (14) (see next section). In the last column we list the references that first reported the detection of the target. All the errors are 1σ unless otherwise mentioned. We also plot the redshift distribution of our sample targets in Figure 2. The majority of the targets are located at $z < 0.1$.

2.2. Absorption Line Analysis

We followed the data reduction process using the standard *XMM*-Newton data analysis software SAS, version 12.0.1[4]. Specifically, we made use the tool *rgsproc* to process the RGS data. We rejected events with flags of "BAD_SHAPE", "ON_BADPIX", "ON_WINDOW_BORDER", and "BELOW_ACCEPTANCE". We also did not keep the cool pixels ("*keepcool* = *no*").

The above procedure outputs three files for each observation: A spectrum, a response file, and a background file. The reduced spectra were then analyzed with the X-ray software package XSPEC

[3]See the NASA Extrgalactic Database at http://ned.ipac.caltech.edu/.

[4]See http://xmm.esa.int/sas/.

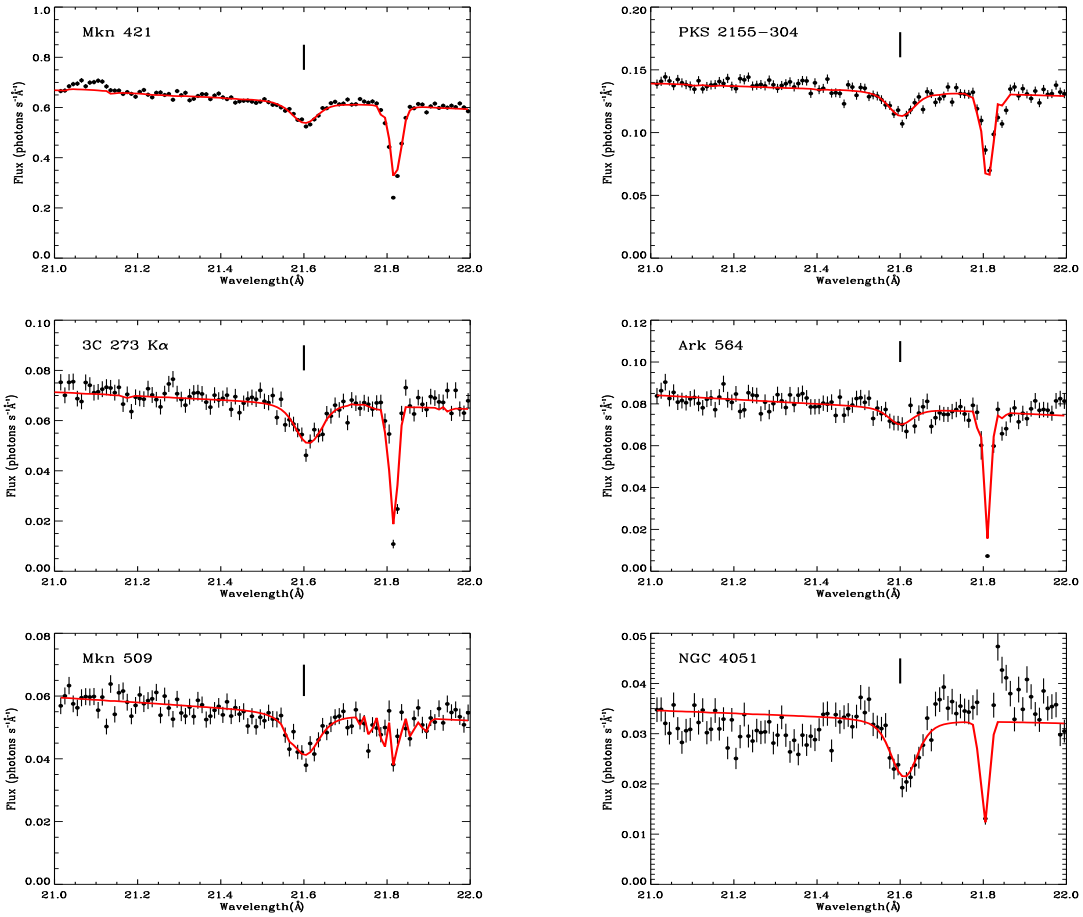

Fig. 3.— RGS spectra of Mkn 421, PKS 2155-304, 3C 273, Ark 564, Mkn 509, and NGC 4051. The location of the O VII K_α line is labeled with a vertical line. The red line in each panel is the model. The structures at 21.82 Å are instrumental features.

version 12.7.1[5]. We fitted the continuum spectrum with a power law plus the absorption by the neutral hydrogen in our Galaxy. Since we are not interested in the broadband spectral properties, we selected only the spectral regions that contain the relevant spectral lines. The He-like oxygen has two transitions, the K_α line at 21.6019 Å and the K_β line at 18.6288 Å (Verner et al. 1996). For most AGNs the K_α line is the only prominent feature, so we performed the fit of the O VII K_α line with a model that was developed in Buote et al. (2009) and discussed also in Fang et al. (2010). We ignored the regions below 21 Å, and above 22 Å, as well as the region around an instrumental feature at $\sim$ 21.8 Å. There are three free parameters in this Voigt-broadened line absorber model: the column density of the absorbing ion, the Doppler-b parameter, and the redshift. This model reflects directly the physical properties of the absorbers and allows the line parameters to be tied

[5]See http://heasarc.nasa.gov/xanadu/xspec/

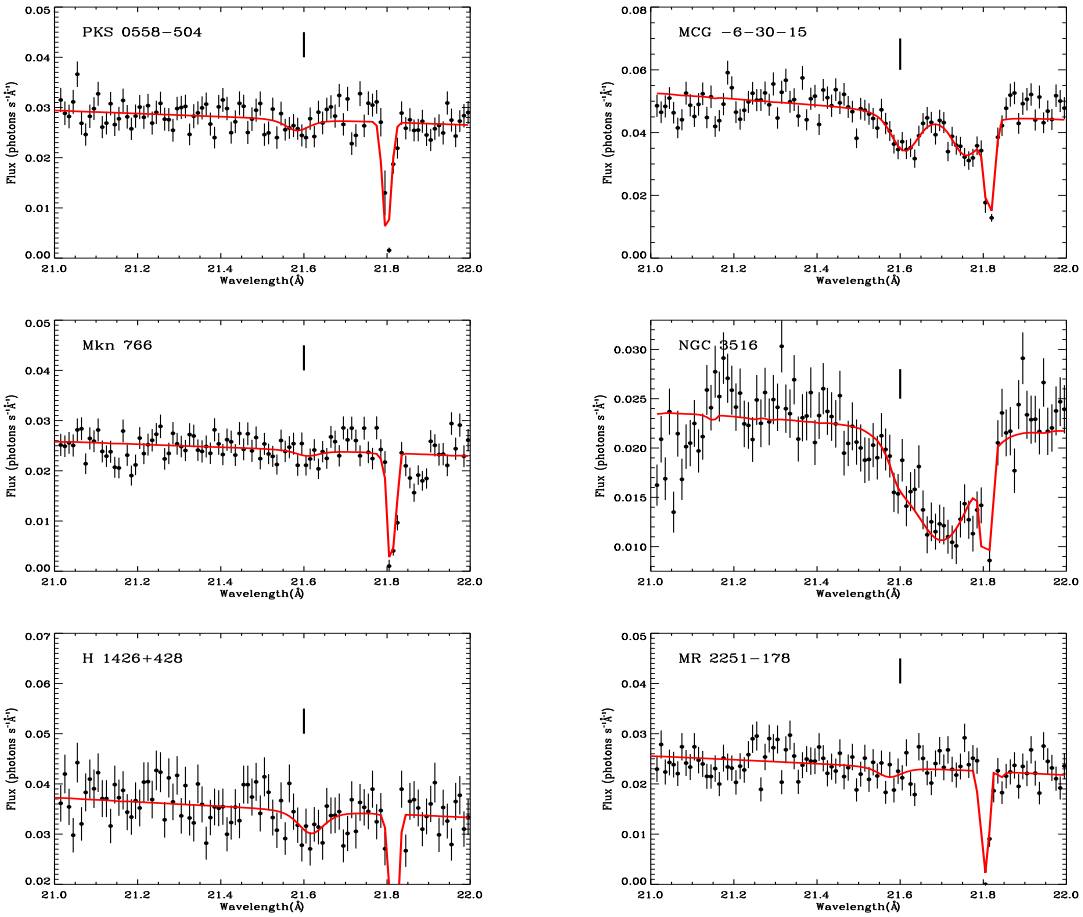

Fig. 4.— Same as the Figure 3, but for RGS spectra for PKS 0558-504, MCG-6-30-15, Mkn 766, NGC 3516, H 1426+428, and MR 2251-178.

consistently between the different spectra. The absolute wavelength uncertainty for RGS is about 100 km s^{-1}.[6], so we limited the line center between with a redshift range of [-0.0004, 0.0004]. This range is also consistent with previous measurements in several high quality spectra. We also limited the Doppler-*b* parameter in the range of 20 to 300 km s^{-1}. The lowest temperature that can still produce a significant fraction of O VII is around 5×10^5 K under collisional ionization, this corresponds to a thermal velocity of ~ 20 km s^{-1}. The upper limit is adopted by assuming the absorbing gas shall not escape from our Galaxy. We performed the fit by minimizing the C-statistic (identical to maximizing the Poisson likelihood function) of Cash (1979), which yields less biased best-fitting parameters (Humphrey et al. 2009).

Figure 3–10 show the spectra of all our targets. Here again we emphasize that the spectra

[6]See XMM-Newton Users Handbook at http://xmm.esac.esa.int/external/xmm_user_support/documentation/uhb/index.html

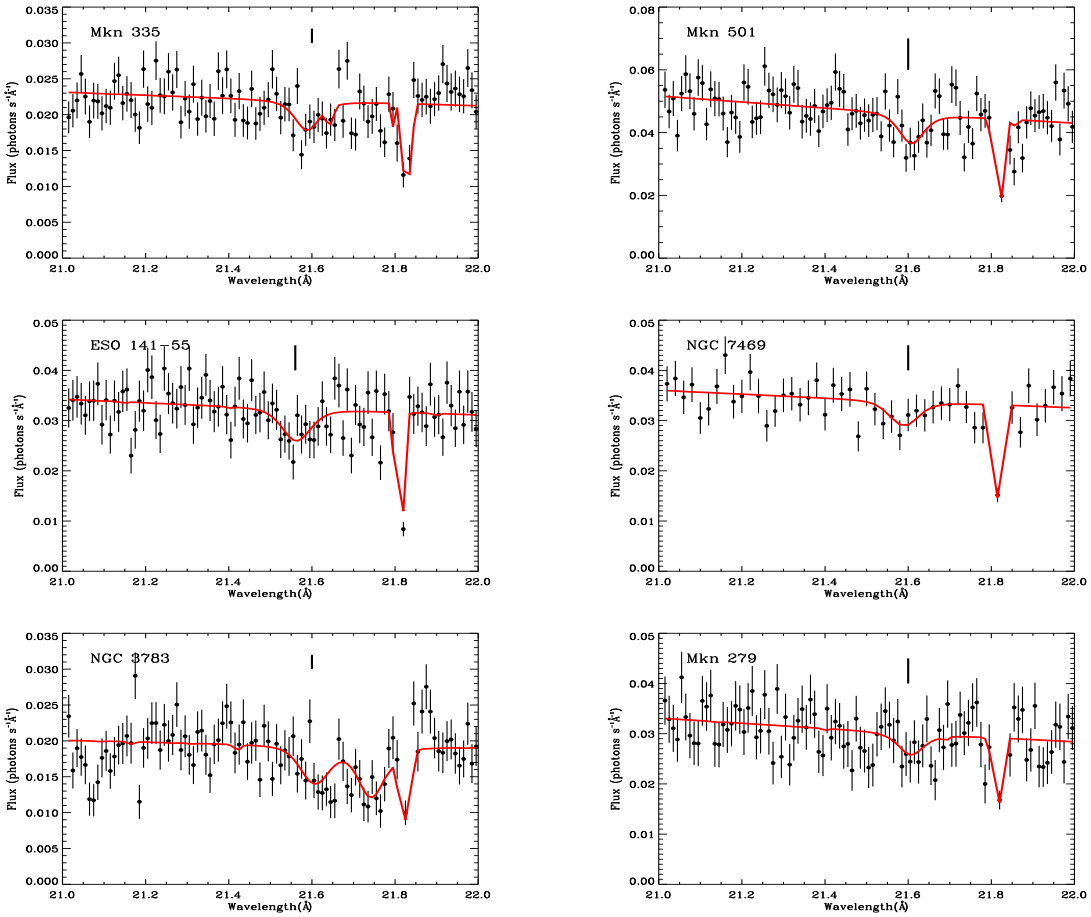

Fig. 5.— Same as the Figure 3, but for Mkn 335, Mkn 501, ESO 141-55, NGC 7469, NGC 3783, and Mkn 279.

for each exposure were combined only for plotting purposes. The red lines are the best-fit model. In fitting the spectra of a target with multiple exposures, we did not co-add the spectra to form a single spectrum and response. Rather, we simultaneously fitted all the exposures, each with its own response. We tied together the three line parameters (column density, Doppler-b parameter, and line center shift) among all the observation for the same target while we let the continuum vary for each observation. This procedure takes longer time to find the best-fit parameters, however, it avoids introducing systematic errors that may arise from co-adding spectra with different responses (see Rasmussen et al. 2007 for details).

Among all the 43 AGN spectra in our sample, the O VII K_α lines of 29 AGNs were discussed previously (see the last column of Table 1). We have included 14 additional AGNs that satisfy our selection criterion. Table 1 columns 9–11 list the three fitting parameters and their 1σ errors. Column (12) is the line equivalent width (EW), and (13) is the significance level. In total 21 targets

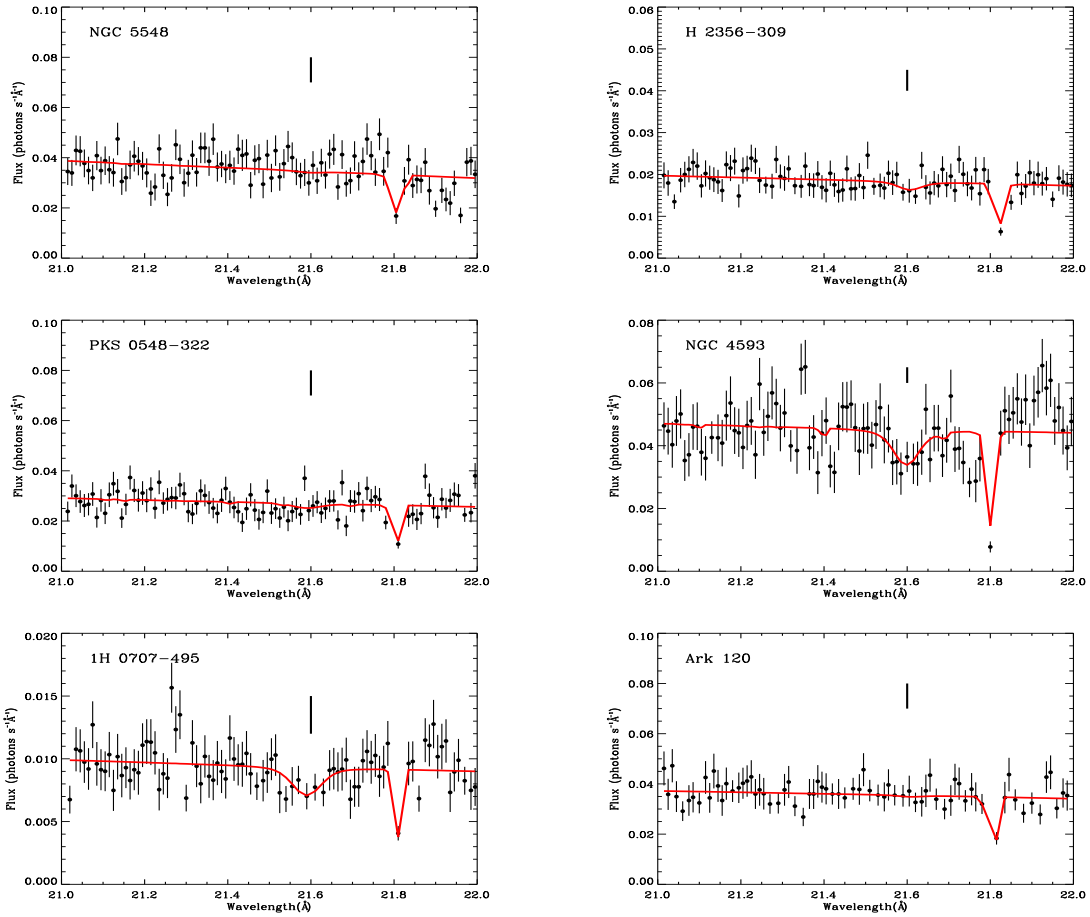

Fig. 6.— Same as the Figure 3, but for NGC 5548, H 2356-309, PKS 0548-322, NGC 4593, 1H 0717-495, and Ark 120.

show the O VII K_α line at more than the 3σ level, among which 7 were first detected in this work[7]. We also list the C-statistic and the degree of freedom in column (14). In Table **??** we listed the detection of O VII $K\alpha$ line at 3, 2, and 1σ for different populations.

For most AGNs we cannot constrain both the Doppler-b parameter and velocity shift of the line center, so we also test another model in which we fix both values: We set the velocity shift of the line center at 0 km s^{-1} and Doppler-b parameter at 100 km s^{-1}. We listed the EW and the significance evaluated with this method in columns (15) and (16), respectively, in Table 1. While we see that both EW and the significance are slightly lower in this method, the results are essentiality consistent with those evaluated by allowing the line parameters to vary within a range. Unless all

[7]We emphasize that the RGS spectra of some of these targets have been analyzed before, but this is the first time that detections of the local O VII K_α lines have been reported.

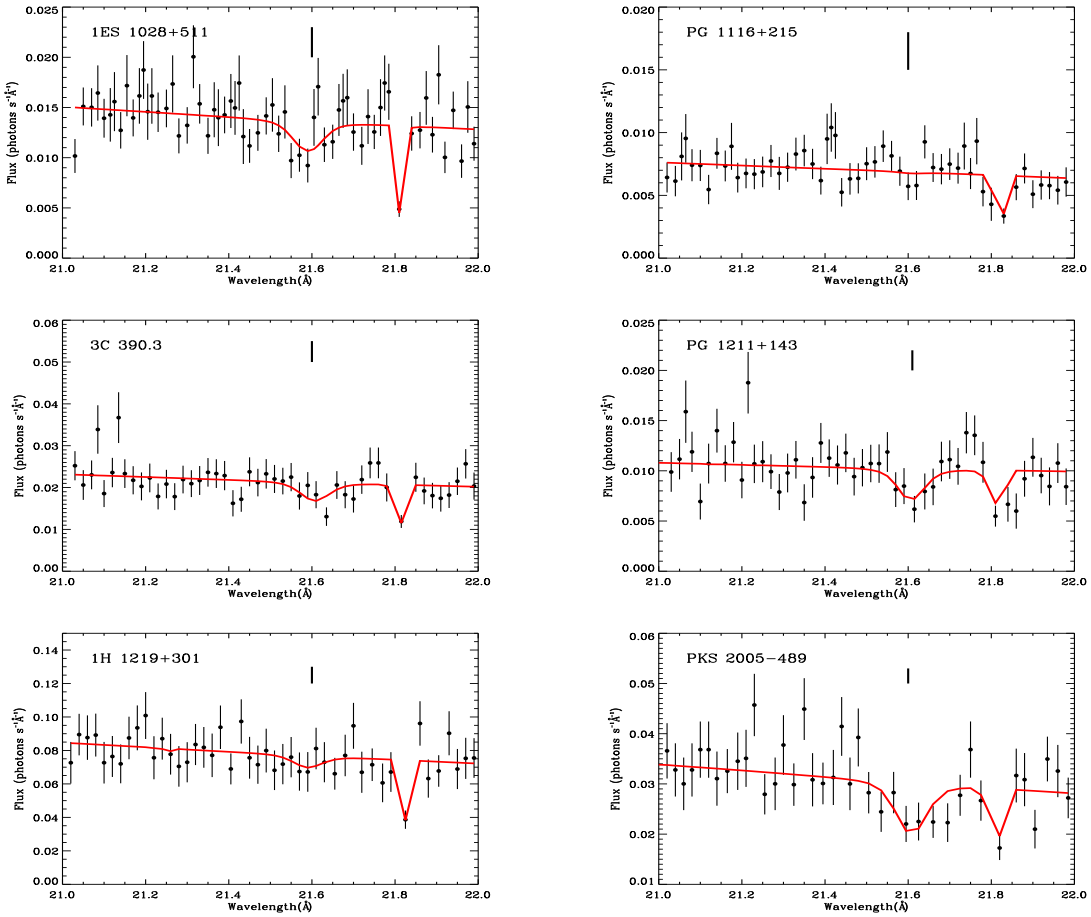

Fig. 7.— Same as the Figure 3, but for 1ES 1028+511, PG1116+215, 3C390.3, PG 1211+143, 1H 1219+301, and PKS 2005-489.

targets in actuality are properly described by these parameters, the derived line significances must be less in general, which is what we find. However, the differences are small and consistent with expectations that a range of b-parameters and velocity shifts are present in the sample.

Our default continuum model is a power law plus the Galactic neutral hydrogen absorption over approximately a 1 Å range centered around the absorption lines of interest. The measured line properties crucially depend on the local continuum model, as well as the wavelength range over which the fitting is performed. To assess whether the power law model would be sufficient to characterize the continuum, we also investigated a more complex model, in particular a cubic-spline, to better match any fine details in the continuum. We found for most targets, such systematic errors are completely dominated by statistical errors. It only becomes important for the first several targets where the statistical errors are much smaller. In the case of Mkn 421, we found with a cubic-spline model the measured O VII Kα line EW is 12.47 ± 0.53 mÅ. This is slightly lower

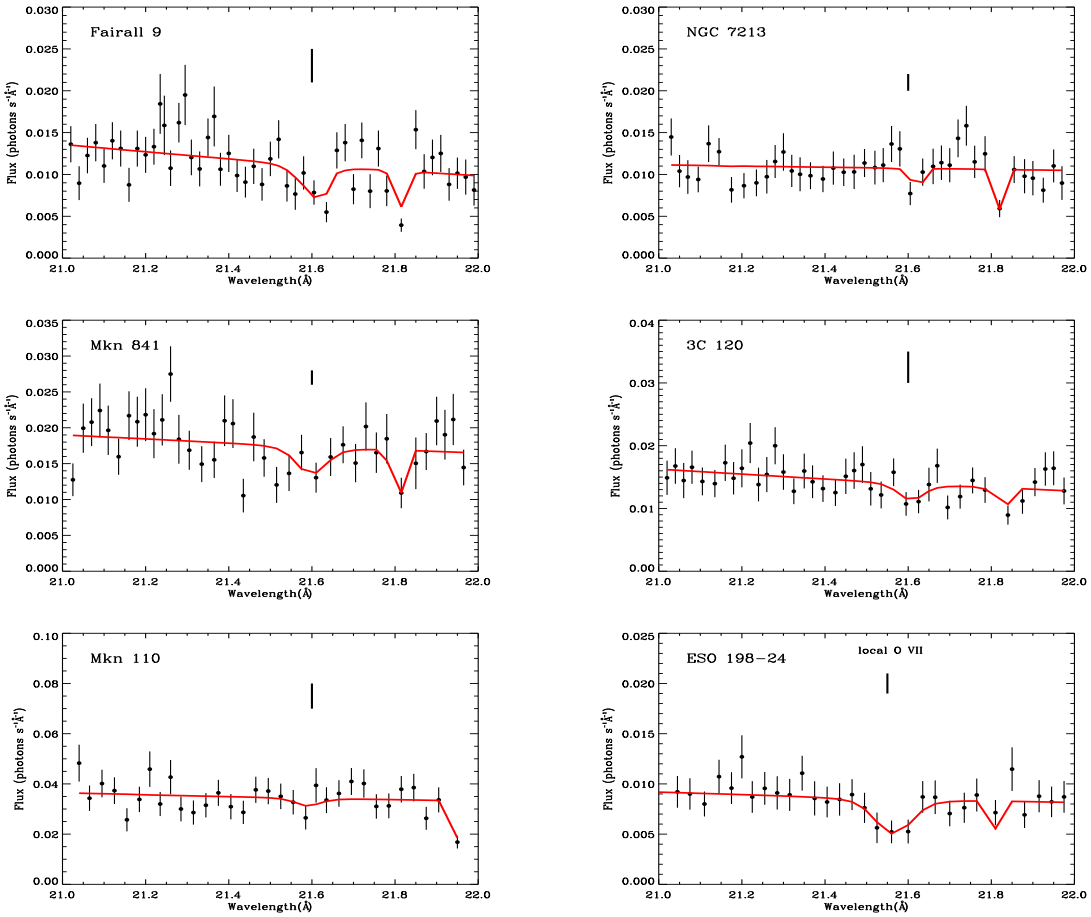

Fig. 8.— Same as the Figure 3, but for Fairall 9, NGC 7213, Mkn 841, 3C 120, Mkn 110, and ESO 198-24.

than what we measured using the single power law model. Such variations are consistent with the large-scale uncertainties in the RGS effective area on 1Å scale (Kaastra et al. 2006). We also tested the systematic errors that may be caused by the wavelength range of our fitting. We found that as long as we restricted our fitting to within a wavelength size of $\sim$ 1Å, the uncertainties caused by systematic errors are negligible.

A potential bias may occur when sometimes the fitting procedure tries to maximum the C-statistics. We tested our procedures by fitting simulated spectra. We define the bias as the difference between the input line EW and mean EW of the simulated spectra. We found in general for strong continuum with highly significant lines, the fitting procedure produced little or no statistically significant bias. For example, in the case of Mkn 421, the ratio between the bias and the standard deviation of the simulated EWs is less than 2%. When the continuum is weaker and the line is less significant, this ratio becomes slightly larger, but in general less than $\sim$ 15%. So our fitting

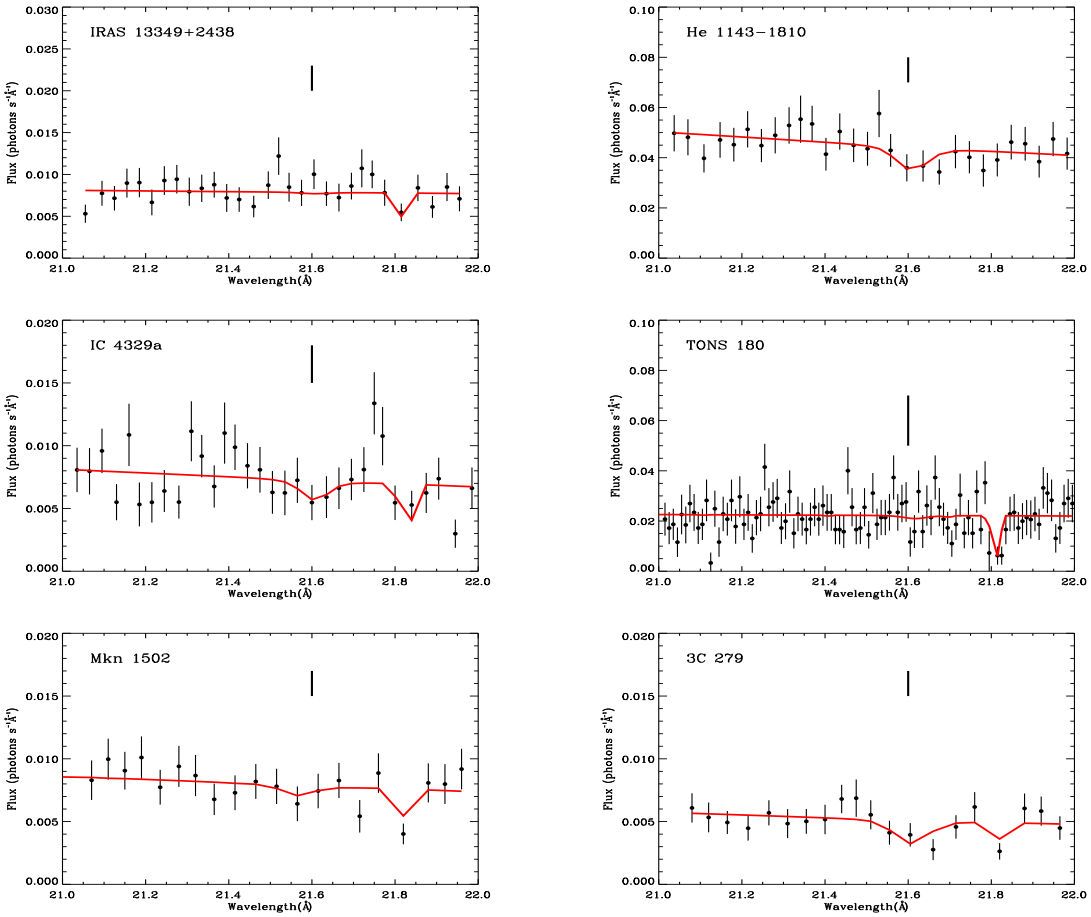

Fig. 9.— Same as the Figure 3, but for IRAS 13349+2438, He 1143-1810, IC 4329a, TONS 180, Mkn 1502, and 3C 279.

procedure shall not produce statistically significant bias.

While our experience indicates that the such a model is often a reasonably good fit to the BL Lac-type targets, in the case of the Seyfert 1 galaxies, absorption features from the warm absorbers can sometimes substantially complicate the analysis, and each case has to be treated differently. We use NGC 3516 as an example here. In Figure 11 we show the combined spectrum of NGC 3516 between 21.2 and 22 Å. This target was observed six times between 2001 and 2006, with a total exposure time of 285 *ksec* (Mehdipour et al. 2010). Here in the plot the data and fit are for illustration purposes only since the actual fit was performed on the individual observation simultaneously. In the left figure we see the broad O VII absorption line produced by the warm absorber intrinsic to the AGN, centered at ~ 21.7 Å. Using the power law plus the broad absorption line as our continuum model, In the bottom panel of the left figure, the $\Delta\chi^2$ plot clearly reveal

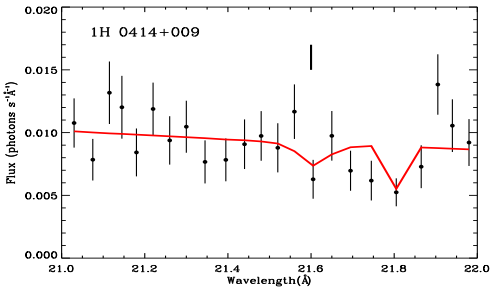

Fig. 10.— Same as the Figure 3, but for 1H 0414+009.

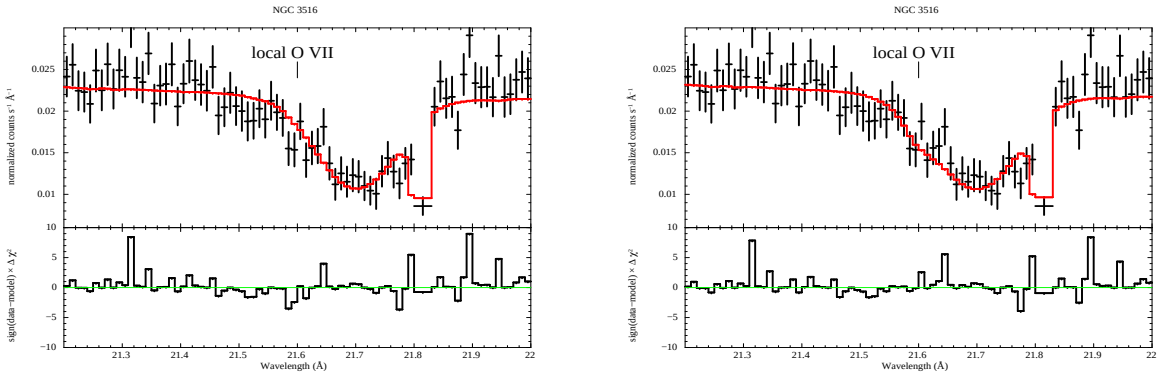

Fig. 11.— Spectra of NGC 3516 between 21.2 and 22 Å before including a $z \sim 0$ O VII K_α absorption line (left figure) and after (right figure). The top panel in each figure is the spectrum, and the bottom is the $\Delta\chi^2$. The structure at ∼21.81 Å is an instrumental feature. The broad absorption feature at ∼21.7 Å is produced by the warm absorber intrinsic to NGC 3516.

the narrow, $z \sim 0$ O VII absorption feature at around 21.6 Å[8]. In the left figure we show the fit after including the local O VII absorption line. The $\Delta\chi^2$ is improved substantially ($\Delta\chi^2 = 11$ for 77 degrees of freedom).

Figure 12 shows the histogram distribution of the O VII K_α Kα line EW (left panel) and column density (right panel). It appears that the most lines have an EW of $\sim$ 20 mÅ, with a range of 10 – 30 mÅ. The column density distribution also centers around $\sim 10^{16}$cm^{-2}, with a range of $10^{15.5}$ – $10^{16.5}$cm^{-2}.

In Figure 13 we show the dependence of the O VII absorption EW on the Galactic longitude (left figures) and latitude(right figures). Red squares and blue circles represent BL Lac and Seyfert

[8]While we use the C-statistics in this paper for less biased parameter fitting, here the conventional χ^2 statistics is adopted to demonstrate the significance of the absorption feature.

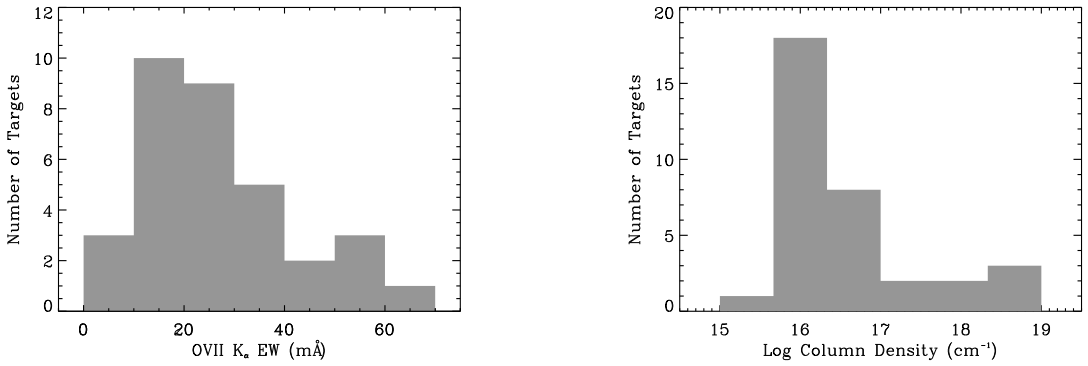

Fig. 12.— Histogram distribution of the O VII K_α line EW (left panel) and column density (right panel).

1 galaxies, respectively. For targets with a detection significance of at least 1σ, we only plot the upper limits. To get a better understanding of the spatial distribution of the O VII absorbers, in the right panels of Figure 13 we divided the targets into two sectors based on their Galactic longitudes: Those close to the Galactic center within 45° (the top right panel of Figure 13) and those more than 45° away from the Galactic center (the middle right panel). The bottom left panel shows the dependence on the Galactic latitide of the entire sample. In the left panel of Figure 13 we also divided the targets into two sectors based on their Galactic latitudes: Those close to the Galactic plane with $|b| < 45°$ (the top left panel of Figure 13) and those that have $|b| > 45°$ (the middle left panel). The bottom left panel shows the dependence on the Galactic longitude of the entire sample.

We have calculated the correlation between the line EW and the Galactic latitude and longitude, using software package ASURV Rev 1.2 (Isobe & Feigelson 1990; LaValley et al. 1992), which implements the methods presented in Isobe et al. (1986). ASURV package is particular useful tool for correlation analysis of censored astronomical data, i.e., non-detections or detection limits (see, e.g., Keane et al. 2014). We listed in Table 3 the probability of correlation by chance for three correlation tests: Cox hazard model, generalized Kendall's tau, and Spearman's rho. A correlation exists if the probability is less than 5%. We have found in general the line EW has no correlation with either the Galactic latitude and the longitude. The only exception is the correlation between the line EW and the Galactic longitude for all the $|b| < 45°$ targets, in which all three tests give probabilities of less than 5%; however, a close look reveals that the correlation is largely dominated by one target, PKS 2005-398. After removal of this target, the probabilities increase to above 5%, and the correlation disappears.

Gupta et al. (2002) suggested that most lines they detected are saturated, leading to larger

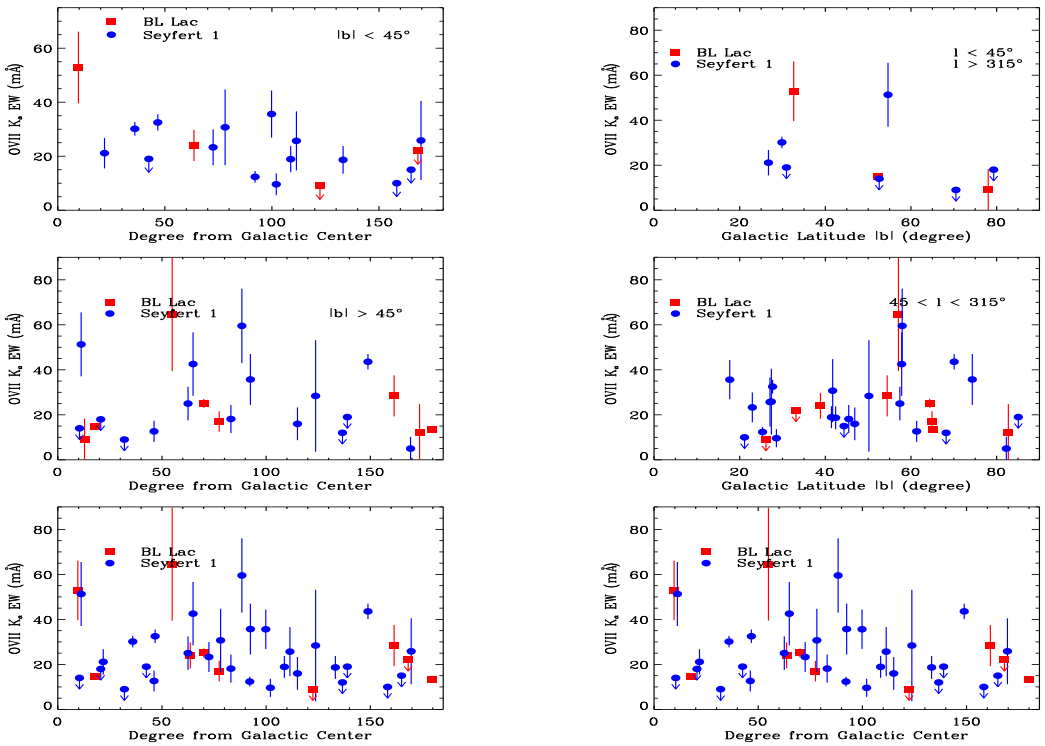

Fig. 13.— O VII K_α line EW as a function of the Galactic longitude (left panels) and latitude (right panels). Red squares and blue circles represent BL Lac and Seyfert 1 galaxies, respectively. For the Galactic latitude plot, the x axis is absolute latitude. For the Galactic longitude plot, the x axis is the angle from the Galactic center. The left panels from top to bottoms are for targets with $|b| < 45°$, $|b| > 45°$, and all samples, respectively. The right panels from the top to bottoms are for targets within 45° from the Galactic center, more than 45° from the Galactic center, and all samples, respectively.

ion column densities in their sample. The Voigt-fitting procedure we adopted allows us to extract directly the column density and Doppler-b parameter information. Our study indicates that at least for the three brightest targets for which we can constrain the Doppler-b parameter, the moderate variation of the Doppler-b parameters demonstrated by Mkn 421 ($b \sim 71$ km s^{-1}), PKS 2155-304 (~ 74 km s^{-1}) and 3C 273 (~ 129 km s^{-1}) does suggest a likely complicate environment for the OVII production. While opacity correction may be important for Mkn 421 and PKS 2155-304 due to their small b values, such correction shall become less important for targets such as 3C 273 with relatively larger b-values. The line saturation may need to be quantified on a case-by-case base when allowed by photon statistics.

In Figure 14 we show the detection rate, or the sky covering fraction, as a function of the source flux. The sky covering fraction is defined as the ratio between the number of detections and

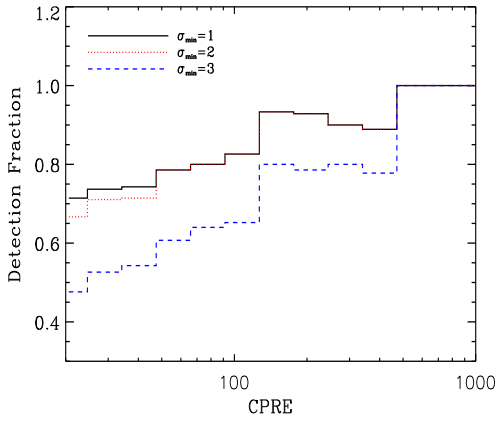

Fig. 14.— Detection rate as a function of the CPRE. The dark solid, red dotted, and blue dashed lines represent the detection rates for lines with at least 1, 2, and 3σ significance. The detection rates increase steadily for all the types to 100% for the brightest targets.

the sample size. The solid black, dotted red, and dashed blue lines are for the detections with at least 3, 2, 1σ significance, respectively. For the 3σ case, the covering fraction increases steadily from $\sim$ 40% for targets with a CPRE of more than 20 counts, to 100% for targets with more than 600 CPRE. For 1σ significance, the covering fraction becomes 100% at $\sim$ 100 CPRE. Our study suggests that the O VII absorbers have a rather uniform distribution in the CGM/ISM.

3. Discussion

3.1. Consistency Check with Previous Work

The detection (or non-detection) of the O VII K_α absorbers in a large fraction of our targets have been reported previously. Here we compare our results with those obtained previously to assess the consistency of our work.

We first compare our results of the three brightest targets (Mkn 421, PKS 2155-304, and 3C 273) with previous work since they have been studied multiple times by different groups, with both *Chandra* and *XMM*-Newton. We focus on the line EW since this is the observable that can be compared directly. We list the values of our work and several previous studies in Table 4. Columns 2, 3, and 4 are EWs measured in this work, with *XMM*-Newton, and with *Chandra*, respectively. Our results are largely consistent with previous work within the error ranges. However, a noticeable difference is that for Mkn 421 and PKS 2155-304, our results are systematically higher than Williams et al. (2005) and Williams et al. (2007) by $\sim$ 30%. While they used *Chandra*, for high quality data like these BL Lacs, such a discrepancy cannot be explained by the systematics between different

instruments (Kaastra et al. 2006). Our results are consistent with Rasmussen et al. (2007), in which they explained in detail the likely cause of this discrepancy with Williams et al. (2005). We refer the readers to this paper for further details.

For the rest of the targets, we mostly compare with results from Bregman & Lloyd-Davies (2007), whose targets consist a subsample of ours. For most detections with more than 1σ significance, our results are consistent with theirs within $\sim 10\%$ or within the error ranges. A few noticeable difference are as follows: In NGC 4051, PKS 0558-504, MR 2251-178, our best-fit values are different from theirs by a factor of 2–3; in NGC 7469 we have a 2.9σ detection while they had a non-detection; in PG 1116+215 we have a non-detection while they detected the O VII K_α line at 2.2σ. Except for NGC 7469, our exposure times are significantly larger than those of Bregman & Lloyd-Davies (2007) (3 – 7 times longer), so our work should have a better statistical precision. For NGC 7469, we do not yet have a clear reason for the discrepancy.

3.2. Galactic Absorbers or AGN Outflows?

Highly ionized, X-ray absorbing gas has been frequently detected in the nearby Seyfert galaxies (see, e.g., Reynolds et al. 1997; Tombesi et al. 2013). While these systems offer an excellent opportunity to probe the inner environment of the AGNs, their presence poses a serious challenge to the study of the CGM/ISM in our Galaxy. These absorbers, in the form of warm absorbers or ultra-fast outflows, often have outflow velocities ranging from a few hundred km s^{-1} to mildly relativistic. Sometimes such a velocity can exactly cancel the redshift effect of the AGN, making the identification of these absorbers particularly difficult. A careful case-by-case study is therefore necessary to determine whether these absorbers are intrinsic to the AGNs or local in the CGM medium in our Galaxy.

In our sample 31 background sources are Seyfert 1 galaxies, among which 20 show the detection of the local O VII K_α line at more than the 2σ level. We made a dedicated study of the warm absorbers reported in these 20 targets. We found 6 Seyfert 1 galaxies have no reported warm absorbers; for the remaining 14 targets, we list them and information regarding their warm absorbers in Table 5 (also see the next subsection for comments on the targets with newly discovered $z \sim 0$ O VII absorption line). Column 1 of Table 5 is the target name; column 2 is the recession velocity; column 3 is the reported velocities for various warm absorber outflows; and the last column is the reference in which the warm absorbers were discussed. We found that in NGC 4051 we do have difficulty separating the local absorber from various components of the warm absorbers. In the case of PG 1211+143, while Pounds et al. (2003) claimed that the O VII K_α line is actually produced by a relativistic outflow with a velocity of $\sim 24,000$ km s^{-1}, Kaspi & Behar (2006) found the absorbers can be explained as a much slower outflow but from other ion species. For all the other cases, it appears outflows cannot compensate the recession velocity, indicating the detected O VII K_α lines are most likely local at $z \sim 0$.

There are further evidence that suggest most of the O VII absorbers should be local to our Galaxy. In a typical complex environment of the AGNs, the warm absorber/ultra-fast outflows are photo-ionized by the AGN, and exhibits absorption features in a variety of ion species in different ionization states. Sometimes emission lines are also detected. These absorbers/emitter typically coexist spatially, and form outflow components with different velocities (see NGC 7469 in our sample). However, for most reported O VII absorbers in our Seyfert 1 galaxy sample, we searched the entire spectrum for each data set and did not find other ion species (except in some cases Ne IX and O VIII) share similar outflowing velocity if assuming they are intrinsic to the AGNs. Such a single-line absorber is unlikely to be produced in the rich environment of an AGN.

3.3. Comments on Individual Target with Newly Discovered Absorption Line

We briefly discuss the targets that have a newly detected, $z \sim 0$ O VII absorber at more than the 2σ level.

Mkn 335 — This is a Seyfert 1 galaxy at $z = 0.0258$. Previously neither X-ray or UV observations showed any intrinsic absorption (see, e.g., Reynolds et al. 1997; Zheng et al. 1995). However, In 2007 and later on, Mkn 335 went into a low state, providing an opportunity to study potential spectral features in its broad-line region (see, e.g, Grupe et al. 2007; Longinotti et al. 2008). Since then *XMM*-Newton observations revealed various outflow components at a velocity of ~ 5000 km s^{-1} (see, e.g., Longinotti et al. 2013), while *Hubble* Space Telescope observations also indicated outflows in ultraviolet with veolcity of ~ 5000 km s^{-1} (see, e.g., Longinotti et al. 2013).

NGC 7469 — This is also a Seyfert 1 galaxy at $z = 0.0169$ (de Vaucouleurs et al. 1991). This target was extensively studied for its ionized outflow and received broadband coverage in optical, ultraviolet and X-ray. Outflows at two main velocity regimes, 600 and 2300 km s^{-1}, were detected in both UV and X-ray observations (see, e.g., Scott et al. 2005; Blustin et al. 2007). Our detected feature at 21.6 Å can also be interpreted as an outflow intrinsic to NGC 7469; however, that would imply a velocity of ~ 5000 km s^{-1}, which would be inconsistent with any of the known outflows. Furthermore, outflows often are associated with multiple features in emission and/or absorption. We examined the spectrum and cannot find any other lines from major ion species with similar velocity. Therefore, we conclude the feature at 21.6 Å is most likely produced by O VII in our Galaxy.

1H 0707-495 — This is a narrow-line Seyfert 1 galaxy at $z = 0.0411$ (Remillard et al. 1986). it is a well-studied target in the X-ray because of its broad iron emission lines that have been interpreted as relativistic emission lines from an ionized accretion disk (Fabian et al. 2009). Lately a mild relativistic highly ionized outflow was also suggested (Dauser et al. 2012). The 21.6 Å absorption feature was first noticed in Blustin & Fabian (2009); however, since they plotted the spectrum in the rest-frame of the AGN, this feature appeared at a wavelength of ~ 20.7 Å, leading them to conclude this is an unknown feature.

PG 1211+143 — This is a bright quasar at $z = 0.0809$ (Marziani et al. 1996). Based on the first ~ 60 *ksec* observation with *XMM*-Newton, Pounds et al. (2003) reported the detection of a high-velocity ionized outflow with velocity around $24,000$ km s^{-1}. Interestingly, as pointed out in McKernan et al. (2004), this velocity can cancel the redshift of the quasar and put the absorber in our Galaxy. Kaspi & Behar (2006) reanalyzed this observation and concluded that most absorption can be explained by a mild outflow with velocity around $3,000$ km s^{-1}. This target was lately observed three more times with *XMM*-Newton. Here our analysis is based on all the four observations with a total exposure time of ~ 218 *ksec*. We confirmed the detection of the 21.6 Å feature. We notice that in the Kaspi & Behar model, while they can identify most high-velocity ion species in Pounds et al. (2003) with a different ion species at a much lower velocity, they still cannot explain the features at 13.45 and 21.6 Å. Coincidently, these are the rest-frame wavelength for the Ne IX and O VII K_α lines, respectively, suggesting these two features may indeed be produced by the hot gas local to the Milky Way.

ESO 198-24 — This is one of the two Seyfert 1 galaxies ($z = 0.0453$) in our sample that have no reported intrinsic absorption or warm absorber (Porquet et al. 2004). The only significant spectral feature that was detected was the Iron K_α line at ~ 6.4 *kev* (see, e.g, Guainazzi et al. 2003).

Mkn 841 — This is also a Seyfert 1 galaxy at ($z = 0.0364$) that has been extensively studied by many X-ray satellites. Its soft excess can be explained either by the reflection from the photoionized disk (Crummy et al. 2006), or as ionized absorption in a relativistic wind (see, e.g., Gierliński & Done 2004; Petrucci et al. 2007). Longinotti et al. (2010) analyzed the high resolution RGS data, and found multiple component warm absorbers with velocities up to ~ 1600 km s^{-1}.

He1143-1810 — This is another Seyfert 1 galaxy ($z = 0.0329$) that has no reported intrinsic absorption or warm absorber. Cardaci et al. (2011) found a broad emission feature centering around 21.45 Å, with a width of ~ 2 Å. They identified this feature as blended O VII emission triplets intrinsic to the source.

1ES 1028+511, PKS 2005-489, and *3C 279* — All three targets are BL Lac-type objects in our sample. For 1ES 1028+511, previous *Chandra* observations with HETGS did not reveal any absorption/emission features (Fang et al. 2005); however, Steenbrugge et al. (2006) later reported tentative detections of narrow absorption features by intervening intergalactic medium, using *Chandra* LETGS and *XMM*-Newton RGS. No emission/absorption features were reported for PKS 2005-489 or 3C 279.

4. Summary

The $z = 0$ O VII absorption lines detected in the X-ray spectra of background AGN have a significant impact on our understanding of the Galactic gas content, both in the distant CGM environment or in the nearby Galactic disk. In this paper, we present an *XMM*-Newton survey of these local O VII absorbers. We summarize our findings here.

- We studied 43 AGNs that satisfy our selection criteria, 12 targets are BL Lac-type, and 31 are Seyfert 1 Galaxies. A total of 21 targets show the detection of the $z = 0$ O VII absorption line with more than the 3σ significance, among which 7 were newly discovered in this work.
- We have fitted the $z = 0$ O VII K_α transition with a Voigt-profile based line model. We find that most K_α lines have an EW of ~ 20 mÅ, with a range of 10 – 30 mÅ. The column density distribution also centers around $\sim 10^{16}\mathrm{cm}^{-2}$, with a range of $10^{15.5}$ – $10^{16.5}\mathrm{cm}^{-2}$.
- We correlate the line equivalent width with the Galactic coordinates and do not find any strong correlations between the line EWs with either the Galactic longitude or latitude.
- The sky covering fraction, defined as the ratio between the number of detections and the sample size, increase from at about 40% for all targets to 100% for the brightest targets, suggesting a uniform distribution of the O VII absorbers.
- Some AGNs have warm absorbers that may complicate the analysis of the local X-ray absorbers. A case-by-case study indicates that while in very few targets we do have difficulty separating local and intrinsic absorbers, for the majority the 21.6 Å absorbers appear to be located in our Galaxy.

The study of the $z = 0$ O VII absorbers plays an important role in understanding the hot gas in and around our Galaxy, since O VII samples a broad range of temperature around 10^6 K. When combined with a study of the x-ray emission, an X-ray absorption study of the Galactic X-ray binaries, as well as a number of other investigations, we expect our study can help provide important clues to the properties of the CGM medium, the multi-phase model of the ISM, as well as questions such as the "missing Galactic baryons". We plan to present our theoretical modeling in a later paper.

We thank the referee for very helpful comments and suggestions. TF was partially supported by the National Natural Science Foundation of China under grant No. 11273021, by "the Fundamental Research Funds for the Central Universities" No. 2013121008, and by the Strategic Priority Research Program "The Emergence of Cosmological Structures" of the Chinese Academy of Sciences, Grant No. XDB09000000. RM was partially supported by the National Natural Science Foundation of China under the grant No. 11333004.

REFERENCES

Blustin, A. J., & Fabian, A. C. 2009, MNRAS, 399, L169

Blustin, A. J., Kriss, G. A., Holczer, T., et al. 2007, A&A, 466, 107

Bregman, J. N. 2007, ARA&A, 45, 221

Bregman, J. N., & Lloyd-Davies, E. J. 2007, ApJ, 669, 990

Buote, D. A., Zappacosta, L., Fang, T., et al. 2009, ApJ, 695, 1351

Cackett, E. M., Miller, J. M., Raymond, J., et al. 2008, ApJ, 677, 1233

Cardaci, M. V., Santos-Lleó, M., Hägele, G. F., et al. 2011, A&A, 530, A125

Cash, W. 1979, ApJ, 228, 939

Crummy, J., Fabian, A. C., Gallo, L., & Ross, R. R. 2006, MNRAS, 365, 1067

Dauser, T., Svoboda, J., Schartel, N., et al. 2012, MNRAS, 422, 1914

de Vaucouleurs, G., de Vaucouleurs, A., Corwin, H. G., et al. 1991, Third Reference Catalogue of Bright Galaxies (New York, NY: Springer New York), 1–632

Dickey, J. M., & Lockman, F. J. 1990, ARA&A, 28, 215

Ebrero, J., Costantini, E., Kaastra, J. S., et al. 2010, A&A, 520, A36

Fabian, A. C., Zoghbi, A., Ross, R. R., et al. 2009, Nature, 459, 540

Fang, T., Bullock, J., & Boylan-Kolchin, M. 2013, ApJ, 762, 20

Fang, T., Buote, D. A., Humphrey, P. J., et al. 2010, ApJ, 714, 1715

Fang, T., Marshall, H. L., Lee, J. C., Davis, D. S., & Canizares, C. R. 2002, ApJ, 572, L127

Fang, T., Mckee, C. F., Canizares, C. R., & Wolfire, M. 2006, ApJ, 644, 174

Fang, T., Sembach, K. R., & Canizares, C. R. 2003, ApJ, 586, L49

Gierliński, M., & Done, C. 2004, MNRAS, 349, L7

Gupta, A., Mathur, S., Krongold, Y., Nicastro, F., & Galeazzi, M. 2012, ApJ, 756, L8

Gupta, A. C., Joshi, U. C., & Fan, J. H. 2002, Ap&SS, 282, 655

Hagihara, T., Yao, Y., Yamasaki, N. Y., et al. 2010, PASJ, 62, 723

Henley, D. B., & Shelton, R. L. 2013, ApJ, 773, 92

Holczer, T., Behar, E., & Arav, N. 2010, ApJ, 708, 981

Humphrey, P. J., Liu, W., & Buote, D. A. 2009, ApJ, 693, 822

Isobe, T., & Feigelson, E. D. 1990, in Bulletin of the American Astronomical Society, Vol. 22, Bulletin of the American Astronomical Society, 917–918

Isobe, T., Feigelson, E. D., & Nelson, P. I. 1986, ApJ, 306, 490

Kaastra, J. S., Werner, N., Herder, J. W. A. d., et al. 2006, ApJ, 652, 189

Kaastra, J. S., Detmers, R. G., Mehdipour, M., et al. 2012, A&A, 539, A117

Kaspi, S., & Behar, E. 2006, ApJ, 636, 674

Kaspi, S., Brandt, W. N., George, I. M., et al. 2002, ApJ, 574, 643

Keane, J. T., Pascucci, I., Espaillat, C., et al. 2014, ApJ, 787, 153

LaValley, M. P., Isobe, T., & Feigelson, E. D. 1992, in Bulletin of the American Astronomical Society, Vol. 24, Bulletin of the American Astronomical Society, 839–840

Longinotti, A. L., Costantini, E., Petrucci, P. O., et al. 2010, A&A, 510, A92

Longinotti, A. L., Krongold, Y., Kriss, G. A., et al. 2013, ApJ, 766, 104

Marziani, P., Sulentic, J. W., Dultzin-Hacyan, D., Calvani, M., & Moles, M. 1996, ApJS, 104, 37

McKernan, B., Yaqoob, T., & Reynolds, C. S. 2004, ApJ, 617, 232

Mehdipour, M., Branduardi-Raymont, G., & Page, M. J. 2010, A&A, 514, A100

Miller, J. M., Raymond, J., Fabian, A. C., et al. 2004, ApJ, 601, 450

Miller, M. J., & Bregman, J. N. 2013, ApJ, 770, 118

Nicastro, F., Zezas, A., Drake, J., et al. 2002, ApJ, 573, 157

Petrucci, P. O., Ponti, G., Matt, G., et al. 2007, A&A, 470, 889

Pounds, K. A., & King, A. R. 2013, MNRAS, 433, 1369

Pounds, K. A., Reeves, J. N., King, A. R., et al. 2003, MNRAS, 345, 705

Rasmussen, A., Kahn, S. M., & Paerels, F. 2003, in Astrophysics and Space Science Library, Vol. 281, The IGM/Galaxy Connection. The Distribution of Baryons at z=0, ed. J. L. Rosenberg & M. E. Putman, 109

Rasmussen, A. P., Kahn, S. M., Paerels, F., et al. 2007, ApJ, 656, 129

Reeves, J. N., Porquet, D., Braito, V., et al. 2013, ApJ, 776, 99

Remillard, R. A., Bradt, H. V., Buckley, D. A. H., et al. 1986, ApJ, 301, 742

Ren, B., Fang, T., & Buote, D. A. 2014, ApJ, 782, L6

Scott, J. E., Kriss, G. A., Lee, J. C., et al. 2005, ApJ, 634, 193

Smith, R. A. N., Page, M. J., & Branduardi-Raymont, G. 2008, A&A, 490, 103

Steenbrugge, K. C., Kaastra, J. S., Blustin, A. J., et al. 2003, A&A, 408, 921

Wang, Q. D., & Yao, Y. 2012, ArXiv e-prints, arXiv:1211.4834

Wang, Q. D., Yao, Y., Tripp, T. M., et al. 2005, ApJ, 635, 386

Williams, R. J., Mathur, S., & Nicastro, F. 2006, ApJ, 645, 179

Williams, R. J., Mathur, S., Nicastro, F., & Elvis, M. 2007, ApJ, 665, 247

Williams, R. J., Mathur, S., Nicastro, F., et al. 2005, ApJ, 631, 856

Yao, Y., & Wang, Q. D. 2005, ApJ, 624, 751

Yao, Y., & Wang, Q. D. 2007, ApJ, 658, 1088

Table 1. The AGN Sample

Name	Type[a]	l	b	z	N_H[b] (10^{20}cm^{-2})	Exposure ($ksec$)	CPRE	Log N(O VII) (cm^{-2})	b (km s^{-1})	Velocity (km s^{-1})	EW (mÅ)	S/N	C/dof	EW (mÅ)	S/N	Note[c]
(1)	(2)	(3)	(4)	(5)	(6)	(7)	(8)	(9)	(10)	(11)	(12)	(13)	(14)	(15)	(16)	(17)
Mkn 421	1	179.832	65.032	0.0300	1.31	929	14554	$16.15^{+0.91}_{-0.34}$	63^{+81}_{-24}	46^{+48}_{-43}	13.13 ± 0.67	19.6	2544/2386	12.95 ± 0.59	21.9	1[d]
PKS 2155-304	1	17.730	-52.246	0.1160	1.71	1086	3591	$16.15^{+1.48}_{-0.39}$	74^{+225}_{-54}	31^{+88}_{-90}	14.82 ± 1.20	12.4	2567/2535	14.83 ± 1.12	13.2	1,2,3
3C 273	1	289.951	64.360	0.1583	1.79	769	1333	$16.52^{+1.48}_{-0.47}$	114^{+185}_{-66}	142^{+90}_{-90}	25.12 ± 2.11	11.9	1728/1692	24.53 ± 1.82	13.5	1,4
Ark 564	2	92.138	-25.337	0.0247	6.38	614	1281	$16.38^{+1.29}_{-0.85}$	45^{+254}_{-25}	24^{+96}_{-144}	12.36 ± 2.18	5.7	691/768	11.92 ± 2.14	5.6	5
Mkn 509	2	35.971	-29.855	0.0344	4.09	876	1254	$17.83^{+0.60}_{-1.73}$	72^{+227}_{-52}	50^{+70}_{-90}	30.15 ± 2.55	11.8	703/738	29.09 ± 2.15	13.5	6
NGC 4051	2	148.883	70.085	0.0023	1.38	677	551	$17.11^{+1.15}_{-0.70}$	159^{+127}_{-56}	120^{+0}_{-49}	43.57 ± 3.43	12.7	562/406	41.28 ± 3.79	10.9	6
PKS 0558-504	2	257.962	-28.569	0.1372	4.55	759	544	$16.95^{+0.70}_{-1.75}$	24^{+275}_{-4}	-118^{+238}_{-2}	9.61 ± 4.03	2.4	458/408	9.46 ± 3.79	2.5	5
MCG -6-30-15	2	313.292	27.680	0.0077	4.09	447	505	$16.57^{+1.96}_{-0.42}$	155^{+144}_{-135}	120^{+0}_{-240}	32.51 ± 3.00	10.8	377/346	32.04 ± 3.35	9.6	7
Mkn 766	2	190.681	82.270	0.0129	1.35	669	401	$15.82^{+1.53}_{-0.82}$	27^{+272}_{-7}	120^{+0}_{-240}	5.00 ± 5.21	1.0	337/299	5.61 ± 4.06	1.4	$\star$
NGC 3516	2	133.236	42.403	0.0088	3.23	481	292	$17.83^{+0.40}_{-2.28}$	20^{+280}_{-0}	-120^{+240}_{-0}	18.66 ± 5.10	3.7	177/136	14.69 ± 4.85	3.0	5
H 1426+428	1	77.487	64.899	0.1291	1.36	312	277	$16.30^{+1.84}_{-0.83}$	75^{+224}_{-55}	120^{+0}_{-227}	17.02 ± 4.56	3.7	166/211	15.33 ± 4.90	3.1	5
MR 2251-178	2	46.197	-61.325	0.0640	2.71	393	250	$15.69^{+2.23}_{-0.69}$	202^{+97}_{-182}	-120^{+240}_{-0}	12.64 ± 4.69	2.7	148/138	11.04 ± 5.47	2.0	5
Mkn 335	2	108.763	-41.424	0.0258	3.99	412	227	$15.90^{+2.30}_{-0.31}$	300^{+0}_{-280}	-81^{+201}_{-39}	18.91 ± 4.87	3.9	274/274	17.80 ± 4.96	3.6	$\star$
Mkn 501	1	63.600	38.859	0.0337	1.74	171	212	$16.75^{+1.62}_{-0.98}$	86^{+213}_{-66}	68^{+52}_{-188}	24.00 ± 5.77	4.2	156/141	22.91 ± 5.18	4.4	8
ESO 141-55	2	338.183	-26.711	0.0371	5.14	232	190	$15.92^{+2.43}_{-0.33}$	300^{+0}_{-280}	-120^{+223}_{-0}	21.13 ± 5.65	3.7	116/136	17.62 ± 5.72	3.1	9
NGC 7469	2	83.099	-45.467	0.0163	4.96	163	140	$15.88^{+2.42}_{-0.49}$	300^{+0}_{-280}	-120^{+240}_{-0}	18.14 ± 6.23	2.9	88/87	16.02 ± 6.62	2.4	5
NGC 3783	2	287.456	22.947	0.0097	9.10	304	137	$16.00^{+2.46}_{-0.37}$	300^{+0}_{-280}	120^{+0}_{-240}	23.30 ± 6.65	3.5	147/103	19.82 ± 6.61	3.0	10
Mkn 279	2	115.042	46.865	0.0305	1.82	173	134	$17.65^{+0.62}_{-2.65}$	20^{+280}_{-0}	120^{+0}_{-240}	15.98 ± 7.28	2.2	101/99	13.62 ± 8.02	1.7	11
NGC 5548	2	31.960	70.496	0.0172	1.83	146	119	...	...	...	< 9	...	...	...	...	...[e]
H 2356-309	1	12.839	-78.035	0.1654	1.33	242	119	$15.97^{+2.11}_{-0.97}$	44^{+255}_{-24}	29^{+91}_{-149}	9.17 ± 9.18	1.0	77/79	9.20 ± 7.40	1.2	12
PKS 0548-322	1	237.566	-26.145	0.0690	2.19	178	117	...	...	...	< 9	...	...	...	...	...
NGC 4593	2	297.483	57.403	0.0090	2.37	103	109	$16.91^{+1.65}_{-1.15}$	89^{+210}_{-69}	-42^{+162}_{-78}	25.00 ± 7.46	3.4	118/78	24.93 ± 7.43	3.4	13
1H 0707-495	2	260.169	-17.672	0.0406	6.06	446	109	$18.43^{+0.38}_{-1.88}$	20^{+280}_{-0}	-120^{+240}_{-0}	35.62 ± 8.73	4.1	67/87	29.46 ± 8.36	3.5	$\star$
Ark 120	2	201.695	-21.131	0.0327	11.86	111	99	...	...	...	< 10	...	...	...	...	...
1ES 1028+511	1	161.439	54.439	0.3604	1.25	251	86	$16.13^{+2.58}_{-0.43}$	300^{+0}_{-280}	-120^{+218}_{-0}	28.41 ± 9.13	3.1	59/69	24.35 ± 9.36	2.6	$\star$
PG 1116+215	2	223.360	68.209	0.1765	1.29	361	68	...	...	...	< 12	...	...	...	...	...
3C 390.3	2	111.438	27.074	0.0561	4.16	117	60	$16.06^{+2.62}_{-0.75}$	300^{+0}_{-280}	120^{+0}_{-240}	25.68 ± 10.93	2.3	31/48	20.13 ± 11.07	1.8	5
PG 1211+143	2	267.552	74.315	0.0809	2.73	218	57	$16.61^{+2.31}_{-0.71}$	173^{+126}_{-153}	120^{+0}_{-240}	35.71 ± 11.30	3.2	62/51	35.89 ± 13.48	2.7	$\star$
1H 1219+301	1	186.359	82.735	0.1836	1.74	29	54	$15.71^{+2.71}_{-0.71}$	300^{+0}_{-280}	-120^{+240}_{-0}	12.28 ± 12.48	1.0	25/40	9.60 ± 12.13	0.8	$\star$
PKS 2005-489	1	350.373	-32.601	0.0710	5.03	62	48	$18.79^{+0.20}_{-1.47}$	20^{+280}_{-0}	120^{+0}_{-240}	52.88 ± 13.28	4.0	39/34	51.60 ± 16.69	3.1	$\star$
Fairall 9	2	295.073	-57.826	0.0470	3.05	162	47	$17.13^{+1.86}_{-1.18}$	156^{+143}_{-136}	-116^{+236}_{-4}	42.55 ± 14.09	3.0	39/32	41.50 ± 16.79	2.5	6
NGC 7213	2	349.588	-52.580	0.0058	2.09	172	47	...	...	...	< 14	...	...	...	...	...
Mkn 841	2	11.209	54.632	0.0364	2.36	111	45	$18.75^{+0.24}_{-1.33}$	20^{+280}_{-0}	-120^{+240}_{-0}	51.31 ± 14.22	3.6	39/35	51.71 ± 16.83	3.1	$\star$

Table 1—Continued

Name	Type[a]	l	b	z	N_H[b] ($10^{20}cm^{-2}$)	Exposure ($ksec$)	CPRE	Log N(O VII) (cm^{-2})	b (km s^{-1})	Velocity (km s^{-1})	EW (mÅ)	S/N	C/dof	EW (mÅ)	S/N	Note[c]
(1)	(2)	(3)	(4)	(5)	(6)	(7)	(8)	(9)	(10)	(11)	(12)	(13)	(14)	(15)	(16)	(17)
3C 120	2	190.373	-27.397	0.0330	10.89	126	44	$16.95^{+1.79}_{-1.69}$	84^{+215}_{-64}	120^{+0}_{-240}	25.84 ± 14.65	1.8	26/34	21.39 ± 12.96	1.7	6
Mkn 110	2	165.011	44.364	0.0353	1.52	47	42	...	...	...	< 15	...	...	...	...	...
ESO 198-24	2	271.639	-57.948	0.0455	3.09	154	31	$18.75^{+0.24}_{-2.69}$	98^{+201}_{-78}	-120^{+218}_{-0}	59.53 ± 16.54	3.6	17/24	61.05 ± 19.23	3.2	⋆
IRAS 13349+2438	2	20.603	79.317	0.1076	1.12	153	31	...	...	...	< 18	...	...	...	...	...
He 1143-1810	2	281.854	41.710	0.0329	3.50	31	31	$16.17^{+2.71}_{-0.75}$	300^{+0}_{-280}	120^{+0}_{-240}	30.71 ± 14.03	2.2	14/24	24.10 ± 15.97	1.5	⋆
IC 4329a	2	317.496	30.920	0.0161	4.38	148	26	...	...	...	< 19	...	...	...	...	5
TONS 180	2	138.995	-85.070	0.0620	1.49	48	26	...	...	...	< 19	...	...	...	...	...
Mkn 1502	2	123.749	-50.175	0.0589	4.94	106	21	$16.75^{+2.23}_{-1.75}$	106^{+193}_{-86}	-120^{+240}_{-0}	28.39 ± 24.78	1.1	16/12	17.00 ± 27.69	0.6	...
3C 279	1	305.104	57.062	0.5362	2.26	152	21	$16.89^{+2.10}_{-0.87}$	299^{+0}_{-279}	120^{+0}_{-240}	64.62 ± 25.15	2.6	12/12	60.93 ± 30.24	2.0	⋆
1H 0414+009	1	191.815	-33.159	0.2870	10.47	90	21	...	...	...	< 22	...	...	...	...	⋆

Note. — (a) 1 – BL Lac, 2 – Seyfert 1; (b) Galactic neutral hydrogen column density (Dickey & Lockman 1990); (c) The references where the $z \sim 0$ O VII absorption line was first reported. A "⋆" sign means the target is first reported in this paper. 1. Rasmussen et al. (2003), 2. Fang et al. (2002), 3. Nicastro et al. (2002), 4. Fang et al. (2003), 5. Bregman (2007), 6. McKernan et al. (2004), 7. Fang et al. (2006), 8. Ren et al. (2014), 9. Miller & Bregman (2013), 10. Williams et al. (2006), 11. Kaspi et al. (2002), 12. Buote et al. (2009), 13. Steenbrugge et al. (2003); (d) For the three brightest targes, Mkn 421, PKS 2155-304, and 3C 273, we did not evalute the line parameters by fixing both the Doppler-b parameter and the line center shift; (e) For targets with a significance of less than 1σ we list the 3σ upper limits of EW.

Table 2. Target Detection

	$> 3\sigma$	$> 2\sigma$	$> 1\sigma$	Total
This work	7	9	11	11
BL Lac	2	3	4	4
Seyfert 1	5	6	7	7
All	21	28	33	43
BL Lac	7	8	10	12
Seyfert 1	14	20	23	31

Note. — Statistics of the detected targets. Top three rows show the detected targets in this work; and bottom three rows show all the targets in our sample. Columns 2, 3, 4 list the targets detected with a S/N larger than 3, 2, and 1σ, respectively. The last column is the total number of targets in each group.

Table 3. Correlation Tests[a]

Correlation	Subsample	Cox Hazard	Kendall Tau	Spearman Rho
EW vs. Degree from GC	$\|b\| < 45°$, BL Lac	6%	7%	10%
	$\|b\| < 45°$, Seyfert 1	14%	29%	22%
	$\|b\| < 45°$, Total	2%	4%	4%
	$\|b\| < 45°$, Total[b]	5%	12%	10%
EW vs. Degree from GC	$\|b\| > 45°$, BL Lac	86%	90%	88%
	$\|b\| > 45°$, Seyfert 1	93%	89%	94%
	$\|b\| > 45°$, Total	89%	98%	90%
EW vs. Degree from GC	BL Lac	33%	22%	22%
	Seyfert 1	44%	47%	46%
	Total	25%	18%	22%
EW vs. $\|b\|$	$l < 45°$ or $l > 315°$, BL Lac	11%	12%	16%
	$l < 45°$ or $l > 315°$, Seyfert 1	28%	40%	27%
	$l < 45°$ or $l > 315°$, Total	7%	17%	13%
EW vs. $\|b\|$	$315 > l > 45°$, BL Lac	46%	83%	87%
	$315 > l > 45°$, Seyfert 1	49%	96%	94%
	$315 > l > 45°$, Total	86%	97%	89%
EW vs. $\|b\|$	BL Lac	82%	39%	61%
	Seyfert 1	16%	56%	56%
	Total	24%	33%	42%

Note. — a. Correlation tests using (1) Cox Hazard, (2) Kendall Tau, and (3) Spearman Rho methods. Columns 3—5 gives the probability that the correlation between eh two parameters is obtained by chance, and a less than 5% probability suggests the two parameters are correlated. b. Total sample excluding the bright BL Lac object PKS 2005-398.

Table 4. Comparison with Previous Observations

Name	This Work (mÅ)	*XMM*-Newton (mÅ)	*Chandra* (mÅ)
Mkn 421	13.13 ± 0.67	13.1 ± 1.0 [1] 11.8 ± 0.8 [3]	11-13 [2] 9.1 ± 1.1 [4]
PKS 2155-304	14.82 ± 1.20	13.7 ± 1.9 [3] 16.3 ± 3.3 [6]	13.3 ± 2.8 [5] 11.6 ± 1.6 [7]
3C 273	25.12 ± 2.11	24.6 ± 3.3 [3] 26.3 ± 4.5 [6]	$28.4^{+12.5}_{-6.2}$ [8]

Note. — [1]: Rasmussen et al. (2007); [2] Kaastra et al. (2006); [3] Bregman & Lloyd-Davies (2007); [4] Williams et al. (2005); [5] Hagihara et al. (2010); [6] Rasmussen et al. (2003); [7] Williams et al. (2007); [8] Fang et al. (2003)

Table 5. Seyfert 1 Galaxies with Warm Absrobers

Name	cz^a (km s^{-1})	Warm Absorber (km s^{-1})	Reference
Ark 564	7472	200–2000	Smith et al. (2008)
Mkn 509	10358	~ 1000	Kaastra et al. (2012)
NGC 4051	800	200–600, 2340, 4600 9000, $0.12c^b$	Pounds & King (2013)
MCG-6-30-15	2610	0, 1900	Holczer et al. (2010)
NGC 3516	2201	~ 100, 1000	Mehdipour et al. (2010)
MR 2251-178	19194	$< 130, \sim 480, 15600$	Reeves et al. (2013)
Mkn 335	7740	5000	Longinotti et al. (2013)
NGC 7469	4619	600, 2300	Blustin et al. (2007)
Mkn 279	9150	0–1500	Ebrero et al. (2010)
NGC 3783	2409	450–750 1360-2080	Kaspi et al. (2002)
NGC 4593	2651	200–600	Steenbrugge et al. (2003)
1H 0707-495	11880	0.11–$0.18c$	Dauser et al. (2012)
PG 1211+143	24450	3000^c	Kaspi & Behar (2006)
		24000^c	Pounds et al. (2003)
Mkn 841	10920	< 1600	Longinotti et al. (2010)

Note. — (a): Recession velocity based on redshift. (b): c is the speed of light. (c): This is one warm absorber, but Kaspi & Behar (2006) and Pounds et al. (2003) have different interpretations.